ADVANCED MATERIALS
www.advmat.de

A Bi_2WO_6-Based Hybrid Photocatalyst with Broad Spectrum Photocatalytic Properties under UV, Visible, and Near-Infrared Irradiation

*Jian Tian, Yuanhua Sang, Guangwei Yu, Huaidong Jiang, Xiaoning Mu, and Hong Liu**

As a free, clean, non-polluting, inexhaustible resource and a domestic energy source, solar energy has long been considered one of the most promising renewable energy sources in the world.[1] In view of solar energy utilization, the search for semiconductor photocatalysts that can harvest the wide spectrum of solar light, from ultraviolet (UV) to near-infrared (NIR) wavelength, and achieve efficient solar energy conversion remains one of the most challenging missions.[2] TiO_2, as a most prominent and suitable material for solar energy harvesting, is widely studied in photocatalysis for the removal of inorganic and organic pollutants.[3] However, TiO_2 possesses a wide band gap of 3.2 eV, allowing the material only to be activated by UV light, which accounts for only 5% of the incoming solar energy.[4] In order to utilize solar energy more efficiently, great efforts have been made to develop visible-light-induced photocatalysts, in which Bi_2WO_6 has attracted a great deal of attention for its good photocatalytic performance in water splitting and organic contaminant decomposition under visible (Vis) light irradiation, which accounts for about 48% of the incoming solar energy.[5,6] Nevertheless, the near-infrared light which accounts for 44% of the solar spectrum, remains unutilized.[7] Over the past 30 years, the search for such near-infrared light photocatalysts has focused mainly on upconversion luminescence of rare earth materials.[7,8] Upon near-infrared excitation at 980 nm, rare earth containing nanoparticles generate upconverted emission peaks ranging from near-infrared to UV or visible spectrum regions. They can serve as an intermedium, which can transfer energy to UV or visible light active photocatalysts to generate the strongly oxidative holes and reductive electrons necessary for the photocatalytic reaction to proceed.[9] However, the efficient utilization of sunlight is limited because of its very narrow absorption band of light at 980 nm.[7,10] Up to now, infrared light active photocatalyst is still a blank area for photocatalysts. Besides up-conversion materials, only a few of near-infrared photocatalysts have been found, such as carbon quantum dots and $Cu_2(OH)PO_4$.[11] Moreover, most promising photocatalysts only possess UV, UV-Vis, Vis-NIR, or NIR photocatalytic activity, separately. They are not compatible to utilize full-spectrum of the solar light. Here we reported a discovery of near-infrared activity of photocatalyst, Bi_2WO_6, which has ever been studied as visible photocatalyst. By assembling Bi_2WO_6 nanosheets on TiO_2 nanobelts, a hybrid nanostructured photocatalyst with enhanced broad spectrum photocatalytic properties has been constructed, which can harness UV, visible, and near-infrared light to decompose organic contaminants in aqueous solution. This suggests its potential as a photofunctional material for waste-water cleaning.

Bi_2WO_6 nanosheets were synthesized by the hydrothermal-co-precipitation method. Bi_2WO_6 with orthorhombic structure belongs to Aurivillius family, which is constructed by alternating $(Bi_2O_2)_n^{2n+}$ layers and perovskite-like $(WO_4)_n^{2n-}$ layers[12] (top right inset of **Figure 1**a). XRD of the samples in this work confirms this Bi_2WO_6 crystal structure (JCPDS No. 79-2381), which is shown in Figure 1a. SEM (top left inset of Figure 1a) and TEM (Figure 1b) images show that the most Bi_2WO_6 nanosheets are square shaped with side length of about 100–200 nm, thickness of about 20 nm. HRTEM image and FFT diffraction pattern (Figure 1c) confirm that the crystal structure of Bi_2WO_6 nanosheets is orthorhombic and the growth direction is (001).

As reported in previous work, Bi_2WO_6 is a good visible light active photocatalyst.[5] In this work, except for the visible photocatalytic property, we found Bi_2WO_6 nanosheet possessed good near-infrared photocatalytic degradation property for methyl orange (MO) (Figure 1f).The degradation rate of MO for Bi_2WO_6 nanosheet under UV, visible, and near-infrared light irradiation for 120 min is 24%, 84% and 58%, respectively. The experiments on degradation ability of light irradiation without photocatalyst involved confirm that all the light irradiation, UV, visible, and near-infrared, could not induce MO degradation (Figure S1 in the Supporting Information). FTIR spectra also suggest that the MO decolorization is due to the photocatalytic reaction of Bi_2WO_6 nanosheets instead of the adsorption. (Figure S2 in the Supporting Information). Although the visible photocatalytic property was confirmed and well-studied, near-infrared photocatalytic property of Bi_2WO_6 has never been reported before. During near-infrared photocatalysis process, a 250 W infrared lamp with a glass filter is used to get near-infrared light spectrum, the spectrum measurement on the filtered near-infrared lamp light showed that the all the possible UV and visible light ($\lambda < 760$ nm) were filtered away (Figure S3 in the Supporting Information), which confirmed the near-infrared photocatalytic activity of Bi_2WO_6 nanosheets. The experiment on photocatalysis cyclic performance of Bi_2WO_6 nanosheets under UV, visible, and near-infrared light irradiation

J. Tian, Y. Sang, G. Yu, Prof. H. Jiang, Prof. H. Liu
State Key Laboratory of Crystal materials
Shandong University
Jinan 250100, P. R. China
E-mail: hongliu@sdu.edu.cn
Dr. X. Mu, Prof. H. Liu
Beijing Institute of Nanoenergy and Nanosystems
Chinese Academy of Science
Beijing 100864, P. R. China

DOI: 10.1002/adma.201302014

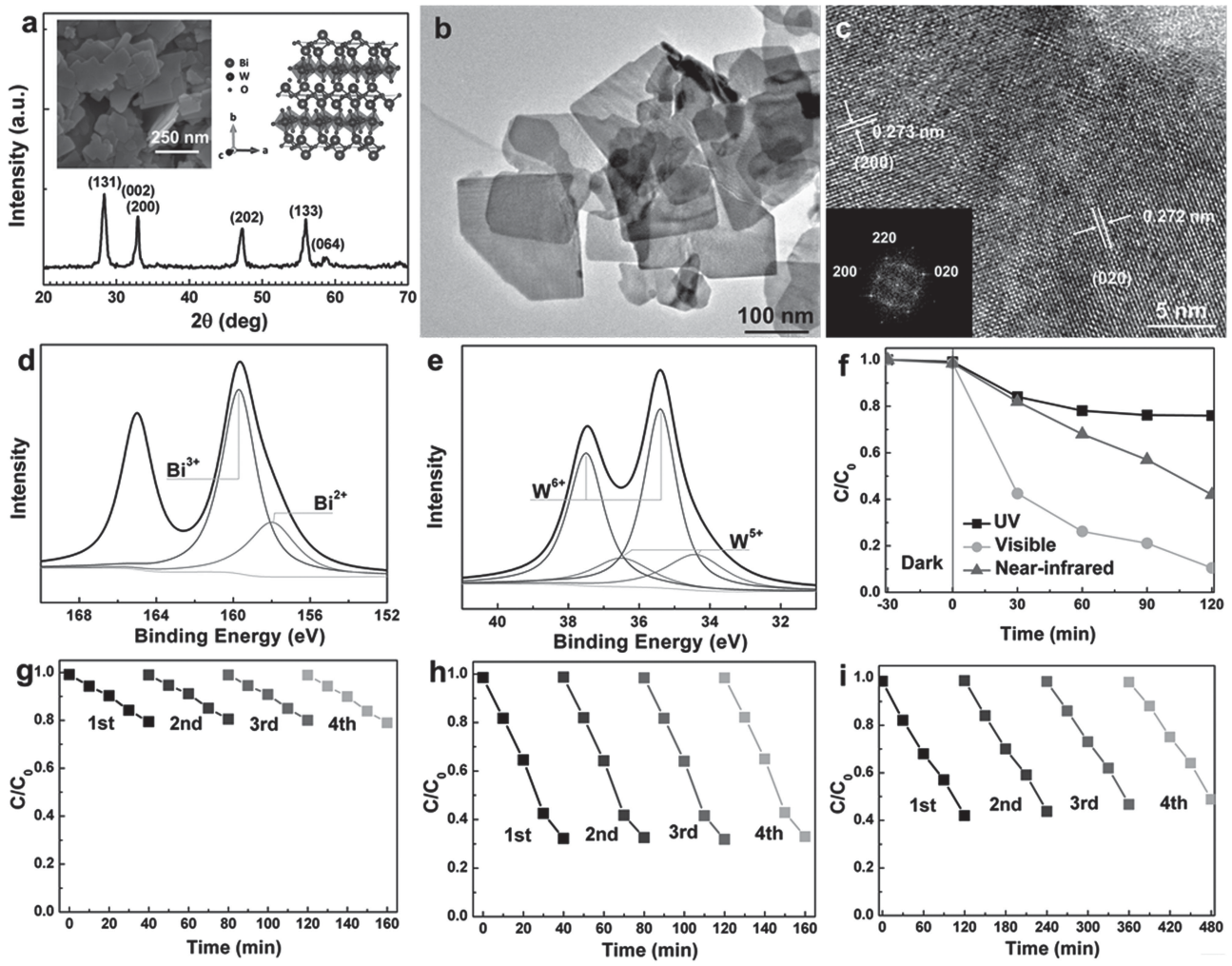

Figure 1. (a) XRD pattern of the Bi_2WO_6 nanosheets. SEM image of Bi_2WO_6 nanosheets is shown in the top left inset. Schematic drawing of the Bi_2WO_6 crystal structure is shown in the top right inset; (b)TEM image of Bi_2WO_6 nanosheets; (c) HRTEM image of Bi_2WO_6 nanosheets and Fourier transform electron diffraction pattern of Bi_2WO_6; Bi_{4f} (d) and W_{4f} (e) core-level XPS spectra of Bi_2WO_6 nanosheet; (f) Photocatalytic degradation of MO in the presence of Bi_2WO_6 nanosheets under UV light, visible light, and near-infrared light irradiation; Irradiation-time dependence of photocatalytic degradation of MO aqueous solution over Bi_2WO_6 nanosheets during repeated photooxidation experiments under (g) UV light, (h) visible light, and (i) near-infrared light irradiation.

demonstrates that the samples exhibit the stable performance, *i.e.* there is no obvious decrease in photocatalytic degradation activity even after four cycles(Figure 1g-i).

X-ray photoelectron spectroscopy (XPS) was used to characterize the valent state of the elements in Bi_2WO_6. Figure 1d shows the Bi4f XPS spectra of Bi_2WO_6 nanosheet. The spin-orbit components of $Bi4f_{5/2}$ consists of peak with binding energies around 165 eV, corresponding to Bi^{3+} in the crystal structure. The feature in the $Bi4f_{7/2}$ spectrum at 159.8 eV is a characteristic peak of the Bi^{3+} ions in Bi_2WO_6. The new feature in the $Bi4f_{7/2}$ spectrum at 158.1 eV could be assigned from the feature of bismuth with a low valence state (Bi^{2+}), and the Bi^{3+}:Bi^{2+} = 71.2%:28.8%. For tungsten, a complex energy distribution of W4f photoelectrons was obtained as shown in Figure 1e. The W4f core-level spectrum could be well fitted into two spin-orbit doublets, corresponding to two different oxidation states of W atoms. The main peaks, having a $W4f_{5/2}$ at 37.5 eV and a $W4f_{7/2}$ at 35.4 eV, are attributed to the W atoms being in a 6+ oxidation state. The second doublet, with a lower binding energy at 34.4 eV and 36.5 eV, results from the emission of $W4f_{5/2}$ and $W4f_{7/2}$ core levels from the atoms in an oxidation state of 5+, in which W^{6+} is 73.7% and W^{5+} is 26.3%.[13] After calculation, the 72-atom super cell of Bi_2WO_6 has three oxygen vacancies. Bi_2WO_6 is rarely noticed before, although its visible photocatalytic property has been intensively studied recent years. However, most recently, Near-infrared light absorption properties $W_{18}O_{49}$ nanomaterials caused by oxygen vacancies has been attracted much attention.[14] Song et al[13b] also discovered that broad infrared fluorescence of bismuth doped germanate glasses, and the broad infrared fluorescence origin from low valence Bi^{2+} ions. The oxygen vacancies of Bi_2WO_6 can act to raise the Fermi level and reduce the band edge, allowing for interband transitions and carrier creation under near-infrared excitation (Figure S4 in the Supporting Information).

Adv. Mater. **2013**,
DOI: 10.1002/adma.201302014

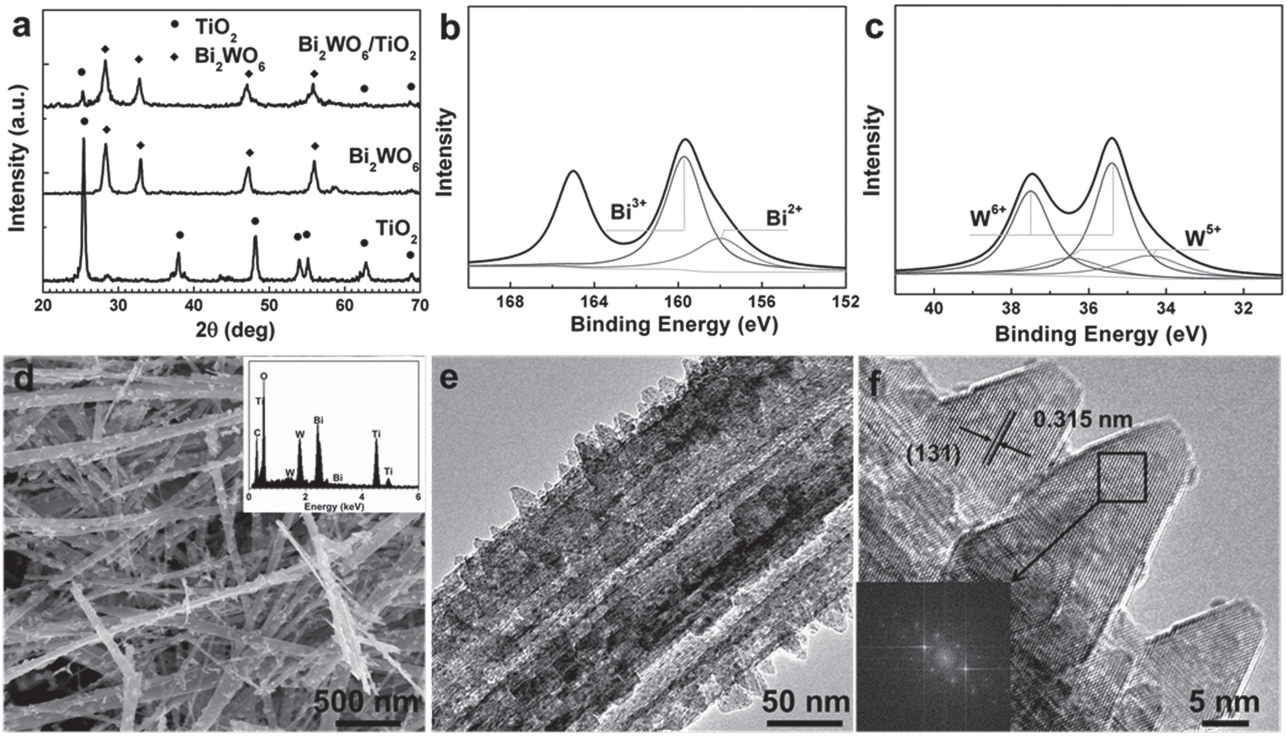

Figure 2. Structural characterization of the Bi_2WO_6/TiO_2 nanobelt heterostructures. XRD patterns (a) of TiO_2 nanobelts, Bi_2WO_6 nanosheets, and Bi_2WO_6/TiO_2 nanobelt heterostructures; Bi_{4f} (b) and W_{4f} (c) core-level XPS spectra of Bi_2WO_6/TiO_2 nanobelt heterostructures; (d) SEM image of Bi_2WO_6/TiO_2 nanobelt heterostructures. Energy-dispersive X-ray spectroscopy (EDS) of Bi_2WO_6/TiO_2 nanobelt heterostructures is shown in the top inset; (e, f) TEM images of Bi_2WO_6/TiO_2 nanobelt heterostructures (14 wt% Bi_2WO_6).

Based on high visible and near-infrared photocatalytic activity of Bi_2WO_6 nanosheets, combining with UV photocatalytic property of TiO_2 nanobelts,[15] a UV-Vis-NIR multi-band hybrid photocatalyst, Bi_2WO_6/TiO_2 nanobelt heterostructures, was synthesized by assembling Bi_2WO_6 nanosheets on surface of TiO_2 nanobelts. The XRD of TiO_2 nanobelts, Bi_2WO_6 nanosheets, and Bi_2WO_6/TiO_2 nanobelt heterostructures (**Figure 2**a) verifies that Bi_2WO_6/TiO_2 nanobelt heterostructures is made up by both anatase TiO_2 (JCPDS les nos.21-1272) and orthorhombic Bi_2WO_6. XPS spectra of Bi_2WO_6/TiO_2 nanobelt heterostructures proves all W^{5+}, W^{6+}, Bi^{2+}, and Bi^{3+} ions exist in the heterostructures, and cause oxygen vacancies (Figure 2b and c), which is similar with Bi_2WO_6 nanosheets. The presence of TiO_2 could not influence the valent state of bismuth and tungsten elements in Bi_2WO_6. The full range of XPS spectra of Bi_2WO_6/TiO_2 and Bi_2WO_6 are shown in Figure S5 in the Supporting Information. Peaks at binding energies corresponding to Bi, W and O are clearly observed, and no impurities other than carbon are observed in the spectra. Energy-dispersive X-ray spectroscopy (EDS) analysis (top inset of Figure 2d) further demonstrates the hybrid nanostructures consisted of Bi, W, Ti and O. In this work, TiO_2 nanobelts were coarsened by acid treatment to enlarge the UV active surface of the nanobelts.[16] SEM and TEM results show that the thickness of the TiO_2 nanobelts is 20-40 nm, the width is 50-200 nm, and the length ranges up to several tens of micrometers (Figure S6 in the Supporting Information). As shown in Figure 2d, after assembling Bi_2WO_6 nanosheets on the surface of TiO_2 nanobelts, the Bi_2WO_6/TiO_2 hybrid nanostructure still keep one-dimensional morphology. Large number of teeth-like Bi_2WO_6 nanosheets with 10–20 nm in width and 20-30 nm in length preferentially grow out from the surface of the TiO_2 nanobelts (Figure 2e and f).The hybrid structure not only provides more visible and near-infrared light absorption sites due to surface of Bi_2WO_6, but also leaves much large space to reserve high UV photocatalytic property due to TiO_2 nanobelts underneath of the teeth root possess high UV light activity.

The lattice on the bottom of teeth-like Bi_2WO_6 nanosheets connect with the lattice of TiO_2 nanobelt surface, and hence a well-defined heterostructure is generated (Figure 2f), which is propitious to charge transmission between two phases. Measuring the distance between two lattice fringes verifies that the resolved interplanar distances are 0.315 nm (Figure 2f), which is consistent with the spacing of (131) planes of orthorhombic Bi_2WO_6.

To prove the photocatalytic activity of the Bi_2WO_6/TiO_2 nanobelt heterostructures, the decomposition of MO in water under UV, visible and near-infrared light irradiation as a function of irradiation time were investigated (**Figure 3**a-c). For comparison, decomposition abilities of Bi_2WO_6 nanosheets, TiO_2 nanobelts, and commercial P25 (anatase 80%, rutile 20%, Degussa Co. Ltd., Germany) were measured under the same experimental conditions. Bi_2WO_6 nanosheets have very limited UV photocatalytic property (Figure 3a). When assembling Bi_2WO_6 nanosheets on the surface of TiO_2 nanobelts, the UV photocatalytic performance of the Bi_2WO_6/TiO_2 nanobelt

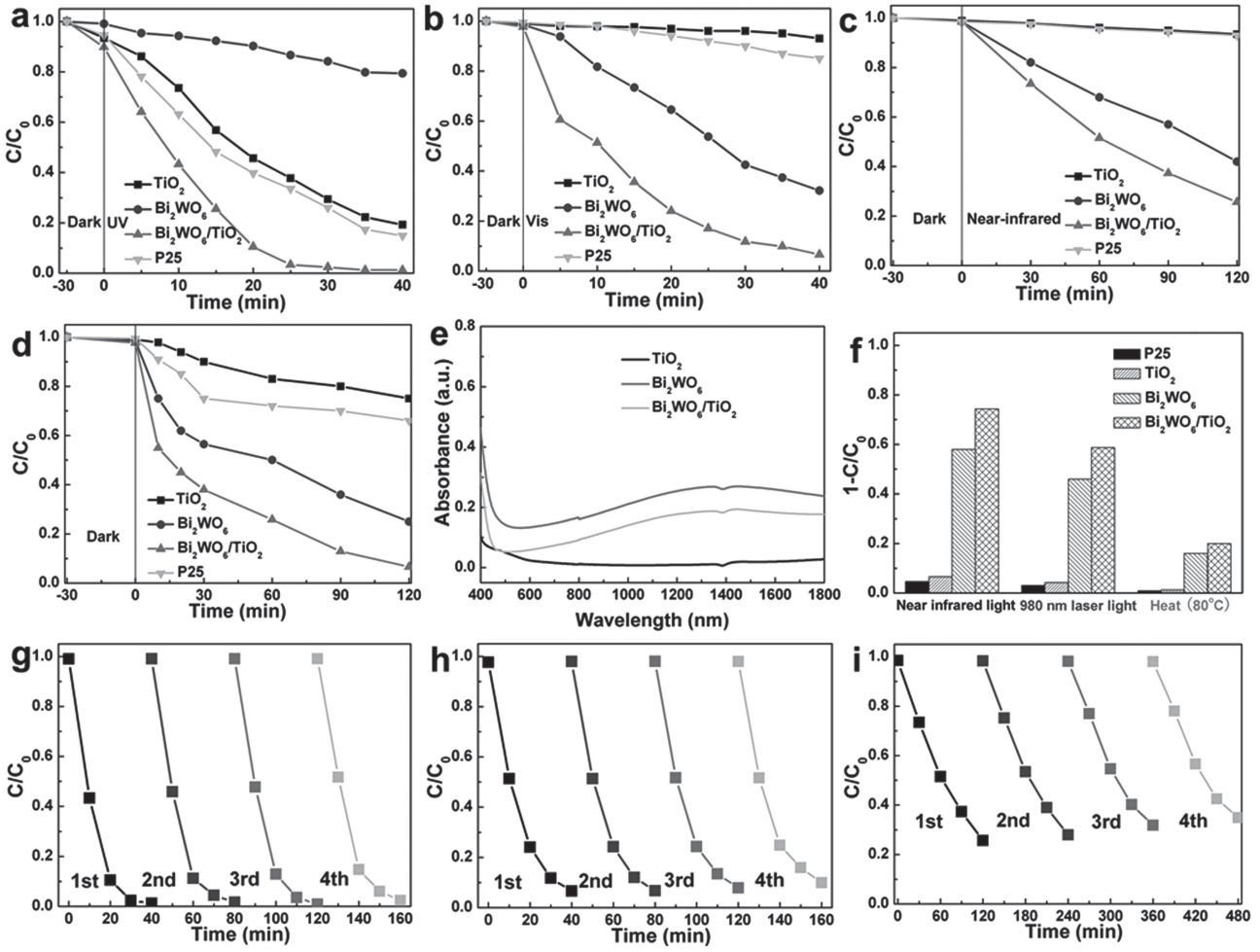

Figure 3. Photocatalytic degradation of MO in the presence of P25, TiO_2 nanobelts, Bi_2WO_6 nanosheets and Bi_2WO_6/TiO_2 nanobelt heterostructures under (a) UV light, (b) visible light, (c) near-infrared light and (d) simulated sunlight irradiation; (e) The experimental visible and near-infrared absorption spectrum of TiO_2 nanobelts, Bi_2WO_6 nanosheets and Bi_2WO_6/TiO_2 nanobelt heterostructures; (f) Photocatalytic degradation of MO in the presence of P25, TiO_2 nanobelts, Bi_2WO_6 nanosheets and Bi_2WO_6/TiO_2 nanobelt heterostructures under near-infrared light irradiation, 980 nm laser light irradiation, and heat at 80 °C in the dark for 120 min; Irradiation-time dependence of photocatalytic degradation of MO aqueous solution over Bi_2WO_6/TiO_2 nanobelt heterostructures (14 wt% Bi_2WO_6) during repeated photooxidation experiments under (g) UV light, (h) visible light, and (i) near-infrared light irradiation.

heterostructures is dramatically improved. The corresponding decomposition rate increases to nearly 100% after 25 min UV irradiation (Figure 3a), which is much higher than that of TiO_2 nanobelts (80.7%), P25(85.1%), and Bi_2WO_6 nanosheets (20.6%), Similar to the results in the previous works,[15] P25, and TiO_2 nanobelts exhibit poor visible photocatalytic activities and Bi_2WO_6 nanosheets possess good visible photocatalytic degradation property. The corresponding MO degradation degree under 40 min visible light irradiation for P25, TiO_2 nanobelts and Bi_2WO_6 nanosheets is 7%, 15% and 67.8%, respectively (Figure 3b). Surprisingly, the photocatalytic performance of the Bi_2WO_6/TiO_2 nanobelt heterostructures is dramatically improved, and the degree of decomposition increases to 100% after visible light irradiation for 40 min.

Bi_2WO_6/TiO_2 nanobelt heterostructures possess enhanced near-infrared photocatalytic activities compared with Bi_2WO_6 nanosheets. The MO degradation degree for Bi_2WO_6 nanosheets and Bi_2WO_6/TiO_2 nanobelt heterostructures under 120 min near-infrared light irradiation is 58% and 74.3%, respectively (Figure 3c). In contrast, P25 and TiO_2 nanobelts have no near-infrared photodegradation ability to MO. The corresponding MO degradation rate for P25 and TiO_2 nanobelts is only 4.1% and 4% in the same conditions. Visible and near-infrared absorption spectrum of TiO_2 nanobelts, Bi_2WO_6 nanosheets and Bi_2WO_6/TiO_2 nanobelt heterostructures confirm that Bi_2WO_6 and Bi_2WO_6/TiO_2 have very broad absorption band, from visible to near-infrared (Figure 3e).The good visible and near-infrared absorption and photocatalytic performance of Bi_2WO_6 nanosheets and Bi_2WO_6/TiO_2 nanobelt heterostructures can attribute to the oxygen vacancies.

As we all know, water itself is a very strong absorber of electromagnetic radiation in the IR region and converts it into heat.[17] Although we use circulating water to cool down the reaction container, the highest temperature of MO solution is

Adv. Mater. 2013,
DOI: 10.1002/adma.201302014

80 °C. The thermocatalytic reference experiment at 80 °C in the dark is carried out. The experimental results (Figure 3f) indicate that the decolorization rate of MO from Bi_2WO_6 nanosheets and Bi_2WO_6/TiO_2 nanobelt heterostructures at 80 °C is 16% and 19%, respectively. These results further confirm that the near-infrared photocatalytic property of Bi_2WO_6 nanosheets and Bi_2WO_6/TiO_2 nanobelt heterostructures is attributed to the photocatalysis reaction, not near-infrared light causes photochemical reaction or temperature effect. We also checked the photocatalytic property of the above catalysts under solar light and 980 nm laser light irradiation, 150W APOLLO solar simulator and 10W 980 nm laser light were used as the light sources. After irradiation of solar light and 980 nm laser light for 120 min, MO degradation rate of Bi_2WO_6 nanosheets and Bi_2WO_6/TiO_2 nanobelt heterostructures is 75% and 93% (Figure 3d), 46% and 58% (Figure 3f), respectively. Similar with Bi_2WO_6 nanosheets, the Bi_2WO_6/TiO_2 nanobelt heterostructures also exhibit the stable photocatalytic performance under UV, visible, and near-infrared light irradiation(Figure 3g-i).

The excellent photocatalytic degradation of MO under UV, visible and near-infrared light irradiation can be partially due to the large specific area of the Bi_2WO_6/TiO_2 nanobelt heterostructures. We evaluated the specific surface area of the prepared samples and the results are shown in Table S1 in the Supporting Information. As can be seen from Table 1, the BET specific surface area of the TiO_2 nanobelt is about 32.236 $m^2\ g^{-1}$, while the specific surface area of the TiO_2 nanobelt treated with acid corrosion increases to 38.572 $m^2\ g^{-1}$. The Bi_2WO_6/TiO_2 nanobelt heterostructure displays a larger specific surface area (about 45.371 $m^2\ g^{-1}$) than Bi_2WO_6 nanosheet (about 35.574 $m^2\ g^{-1}$), P25 (about 43.401 $m^2\ g^{-1}$) and TiO_2 nanobelt, which leads to the exposure of more active sites giving high photocatalytic activity. An obvious decrease of the photoluminescence of the Bi_2WO_6/TiO_2 nanobelt heterostructures can be observed as compared with that of TiO_2 nanobelts or Bi_2WO_6 nanosheets alone, indicating that the coupling of TiO_2 and Bi_2WO_6 in the heterostructures effectively diminish the recombination of photoinduced electron-hole pairs, which is beneficial to the photocatalytic activity. (Figure S7 in the Supporting Information)

In summary, near-infrared light photocatalytic activity of Bi_2WO_6 nanosheets was firstly found. The high near-infrared excitation of Bi_2WO_6 can attribute to the oxygen vacancies. Bi_2WO_6/TiO_2 nanobelt heterostructures synthesized through an economic and practical hydrothermal method possessed the enhanced UV, visible and near-infrared photocatalytic activity. This result is of significance in the utilization of all solar band energy, especially for near-infrared light, which constitutes a considerable part of sunlight. The photocatalytic efficiency of Bi_2WO_6/TiO_2 could be enhanced by hetero-integration of these materials, as well as high specific surface area of the Bi_2WO_6/TiO_2 hybrid nanobelt heterostructures. There will be better ways to take advantage of solar energy in the future.

Experimental Section

TiO_2 nanobelts were synthesized through a hydrothermal procedure. Typically, 0.1 g of P25 powders was mixed with 20 mL of an aqueous solution of 10 M NaOH, followed by a hydrothermal treatment at 180 °C in a 25 mL Teflon-lined autoclave for 48 h. The treated powders were washed thoroughly with deionized water followed by a filtration and drying process. The obtained sodium titanate nanobelts were then immersed in an aqueous solution of 0.1 M HCl for 48 h and then washed thoroughly with water to produce $H_2Ti_3O_7$ nanobelts. The $H_2Ti_3O_7$ nanobelts were added into a 25 mL Teflon vessel, which was filled with an aqueous solution of 0.02 M H_2SO_4 up to 80% of the total volume and maintained at 100 °C for 12 h. Finally, the products were isolated from the solution by centrifugation and sequentially washed with deionized water for several times, and dried at 70 °C for 10 h. Thermal annealing of the acid-corroded $H_2Ti_3O_7$ nanobelts at 600 °C for 2 h led to the production of TiO_2 nanobelts with roughened surfaces.

Bi_2WO_6/TiO_2 nanobelt heterostructures with various mole ratios from 1:12 to 4:12 were prepared by a simple hydrothermal-co-precipitation method. In a typical reaction, 0.2-0.8 mmol of $Bi(NO_3)_3{\cdot}5H_2O$ and 0.1-0.4 mmol of $Na_2WO_4{\bullet}2H_2O$ were mixed together in 40 mL of ethylene glycol or nitric acid to form the homogeneous solution. Then 1.2 mmol of TiO_2 nanobelts were dispersed into the above solution and then added into the Teflon-lined autoclave. The autoclave was sealed and heated to 160 °C for 15 h. The product was washed with deionized water and ethanol to remove any ionic residual, then dried in oven at 70 °C for 12 h. For comparison, Bi_2WO_6 nanosheets were also prepared in a similar process excepting for without TiO_2 nanobelts.

X-ray powder diffraction (XRD) patterns of the samples were recorded on a Bruke D8 Advance powder X-ray diffractometer with Cu Kα (λ = 0.15406 nm). A HITACHI S-4800 field emission scanning electron microscope (FE-SEM) was used to characterize the morphologies of the synthesized samples, and the chemical composition was examined via energy-dispersive X-ray spectroscopy (EDS) attached to the FE-SEM. High resolution transmission electron microscopic (HRTEM) images were acquired with a JOEL JEM 2100 microscope. UV-Vis-NIR diffuse reflectance spectra (DRS) of the samples were recorded on a UV-Vis-NIR spectrophotometer (Cary 5000, Varian) with an integrating sphere attachment within the range of 200 to 2000 nm and with $BaSO_4$ as the reflectance standard. X-ray photoelectron spectroscopy (XPS) was performed using an ESCALAB 250. The specific surface area was calculated using the Brunauer-Emmett-Teller (BET) method using the measurement instrument (Micromeritics, ASAP2020).

The photocatalytic activity of the Bi_2WO_6/TiO_2 nanobelt heterostructures was investigated by the photodegradation of methyl orange (MO, 20 mg/L). In a typical measurement, 20 mL of an aqueous suspension of MO and 20 mg of the heterostructure powders were placed in a 50 mL beaker. Prior to photoirradiation, the suspensions were magnetically stirred in the dark for 30 min to establish adsorption-desorption equilibrium between the dye and the surface of the catalysts under ambient conditions. A 350 W mercury lamp with a maximum emission at 356 nm was used as the UV source, a 300 W Xe arc lamp as the visible light source where the UV components were filtered out during visible light photocatalysis, a 250 W infrared lamp as the near-infrared light source where the $\lambda < 760$ nm were filtered out during near-infrared light photocatalysis, and a 150W APOLLO solar simulator was used as the solar light source. At varied irradiation time intervals, an aliquot of the mixed solution was collected and centrifuged, and the residual MO concentration in the supernatant was analyzed by UV-vis spectroscopic measurements (Hitachi UV-3100).

Supporting Information

Supporting Information is available from the Wiley Online Library or from the author.

Acknowledgements

The authors are thankful for funds from National Natural Science Foundation of China (NSFDYS: 50925205, 50990303 and 51002089), Innovation Research Group (IRG: 51021062), the Program of Introducing

Talents of Discipline to Universities in China (111 Program b06015) and the "100 Talents Program" of Chinese Academy of Sciences.

Received:
Revised:
Published online:

[1] a) T. P. Yoon, M. A. Ischay, J. Du, *Nat. Chem.* **2010**, *2*, 527; b) Q. Xiao, J. Zhang, C. Xiao, Z. Si, X. Tan, *Sol. Energy* **2008**, *82*, 706; c) X. Chen, C. Li, M.Grätzel, R Kostecki, S S. Mao, *Chem. Soc. Rev.* **2012**, *41*, 7909; d) Y. Bai, H. Yu, Z. Li, R.Amal, G. Q. Lu, L. Wang, *Adv. Mater.* **2012**, *24*, 5850; e) H. Zhang, Y. Wang, D. Yang, Y. Li, H. Liu, P. Liu, B. J. Wood, H. Zhao, *Adv. Mater.* **2012**, *24*, 1598; f) K. Park, Q. Zhang, B. B. Garcia, X. Zhou, Y. H. Jeong, G. Cao, *Adv. Mater.* **2010**, *22*, 2329.

[2] a) Y. Wang, G. Du, H. Liu, D. Liu, S. Qin, N. Wang, C. Hu, X. Tao, J. Jiao, J. Wang, *Adv. Funct. Mater.* **2008**, *18*, 1131; b) J. Yuan, X. Liu, O. Akbulut, J. Hu, S. L. Suib, J. Kong, F. Stellacci, *Nature Nanotech.* **2008**, *3*, 332; c) S. K. Cushing, J. Li, F. Meng, T. R. Senty, S. Suri, M. Zhi, M. Li, A. D. Bristow, N. Wu, *J. Am. Chem. Soc.* **2012**, *134*, 15033; d) X. Wu, Z. Chen, G. Q. Lu, L. Wang, *Adv. Funct. Mater.* **2011**, *21*, 4166; e) Q. Zhang, C. S. Dandeneau, X. Zhou, G. Cao, *Adv. Mater.* **2009**, *21*, 4087.

[3] a) C. Chen, W. Ma, J. Zhao, *Chem. Soc. Rev.* **2010**, *39*, 4206; b) Z. Xiong, X. S. Zhao, *J. Am. Chem. Soc.* **2012**, *134*, 5754; c) Q. Wang, M. Zhang, C. Chen, W. Ma, J. Zhao, *Angew. Chem. Int. Ed.* **2010**, *49*, 7976; d) X. Chen, L. Liu, P. Y. Yu, S. S. Mao, *Science* **2011**, *331*, 746.

[4] a) M. Murdoch, G. Waterhouse, M. Nadeem, J. Metson, M. Keane, R. Howe, J. Llorca, H. Idriss, *Nature Chem.* **2011**, *3*, 489; b) A. Hagfeldt, M. Gratzel, *Chem. Rev.* **1995**, *95*, 49.

[5] J. Tang, Z. Zou, J. Ye, *Catal. Lett.* **2004**, *92*, 53.

[6] a) G. Li, D. Zhang, J. C. Yu, M. K. H. Leung, *Environ. Sci. Technol.* **2010**, *44*, 4276; b) F. Amano, K. Nogami, B. Ohtani, *J. Phys. Chem. C* **2009**, *113*, 1536; c) F. Amano, A. Yamakata, K. Nogami, M. Osawa, B. Ohtani, *J. Am. Chem. Soc.* **2008**, *130*, 17650.

[7] W. Qin, D. Zhang, D. Zhao, L. Wang, K. Zheng, *Chem. Commun.* **2010**, *46*, 2304.

[8] a) S. Zhuo, M. Shao, S. T. Lee, *ACS nano* **2012**, *6*, 1059; b) W. Zou, C. Visser, J. A. Maduro, M. S. Pshenichnikov, J. C. Hummelen, *Nature Photon.* **2012**, *6*, 560.

[9] a) F. Wang, Y. Han, C. S. Lim, Y. Lu, J. Wang, J. Xu, H. Chen, C. Zhang, M. Hong, X. Liu, *nature* **2010**, *463*, 1061; b) G. S. Yi, G. M. Chow, *Adv. Funct. Mater.* **2006**, *16*, 2324.

[10] a) F. Wang, J. Wang, X. Liu, *Angew. Chem. Int. Ed.* **2010**, *122*, 7618; b) Z. X. Li, F. B. Shi, T. Zhang, H. S. Wu, L. D. Sun, C. H. Yan, *Chem. Commun.* **2011**, *47*, 8109; c) C. Li, F. Wang, J. Zhu, J. C. Yu, *Appl. Catal. B: Environ.* **2010**, *100*, 433.

[11] a) H. Li, R. Liu, Y. Liu, H. Huang, H. Yu, H. Ming, S. Lian, S. T. Lee, Z. Kang, *J. Mater. Chem.* **2012**, *22*, 17470; b) C. Pak, J. Y. Woo, K. Lee, W. D. Kim, Y. Yoo, D. C. Lee, *J. Phys. Chem. C* **2012**, *116*, 25407; c) Y. Nishijima, K. Ueno, Y. Kotake, K. Murakoshi, H. Inoue, H. Misawa, *J. Phys. Chem. Lett.* **2012**, *3*, 1248; d) G. Wang, B. Huang, X. Ma, Z. Wang, X. Qin, X. Zhang, Y. Dai, M. H. Whangbo, *Angew. Chem. Int. Ed.* **2013**, *52*, 4810.

[12] a) Y. Li, J. Liu, X. Huang, *Nanoscale Res. Lett.* **2008**, *3*, 365; b) N. Kim, R. N. Vannier, P. Clare, *Chem. Mater.* **2005**, *17*, 1952.

[13] a) S. Jeon, K. Yong, *Nanotechnology* **2007**, *18*, 245602; b) Z. Song, D. Zhou, Z. Yang, Z. Yin, R. Wang, J. Shang, K. Lou, Y. Xu, Y. Hu, J. Qiu, *J. Chin. Ceramic Soc.* **2010**, *11*, 023.

[14] G. Leftheriotis, S. Papaefthimiou, P. Yianoulis, A. Siokou, *Thin solid films* **2001**, *384*, 298.

[15] W. Zhou, G. Du, P. Hu, G. Li, D. Wang, H. Liu, J. Wang, R. I. Boughton, D. Liu, H. Jiang, *J. Mater. Chem.* **2011**, *21*, 7937.

[16] W. Zhou, L. Gai, P. Hu, J. Cui, X. Liu, D. Wang, G. Li, H. Jiang, D. Liu, H. Liu, *Cryst Eng Comm* **2011**, *13*, 6643.

[17] B. Wozniak, J. Dera, in *Light absorption in sea water*, Vol. *33*, Springer, **2007**.